Journal of
Mechanics of
Materials and Structures

A DIELECTRIC BREAKDOWN MODEL FOR AN INTERFACE CRACK IN A PIEZOELECTRIC BIMATERIAL

Yuri Lapusta, Alla Sheveleva, Frédéric Chapelle and Volodymyr Loboda

Volume 15, No. 1 January 2020

msp

JOURNAL OF MECHANICS OF MATERIALS AND STRUCTURES
Vol. 15, No. 1, 2020
dx.doi.org/10.2140/jomms.2020.15.87

A DIELECTRIC BREAKDOWN MODEL FOR AN INTERFACE CRACK IN A PIEZOELECTRIC BIMATERIAL

YURI LAPUSTA, ALLA SHEVELEVA, FRÉDÉRIC CHAPELLE AND VOLODYMYR LOBODA

A mode III electrically conductive crack between two piezoelectric semi-infinite spaces under the action of anti-plane mechanical loading and in-plane electrical field parallel to the crack faces is considered. All electromechanical quantities are presented as piecewise analytic vector functions. The problem is solved analytically, revealing an oscillating singularity at the crack tips in the stress and electric fields. To eliminate the electric field singularity the dielectric breakdown (DB) model is applied. According to this model, the electric field along some zone of the crack continuation is initially assumed to be equal to the electric breakdown strength and the length of this zone remains still unknown. A nonhomogeneous combined Dirichlet–Riemann boundary value problem for the crack with DB zone is formulated. An exact analytical solution of this problem is presented and the DB zone length is found from the electric field finiteness at the end point of this zone. The simple transcendental equation with respect to DB zone length is solved numerically and all required electromechanical quantities are found in closed analytical form. The DB model for a crack in a homogeneous material is also considered and compared with known results.

1. Introduction

Ferroelectric ceramics are widely used in piezoelectric devices, such as sensors, resonators and actuators, due to their distinctive piezoelectric propertyies. However, ferroelectric ceramics are brittle and susceptible to cracking at all scales. Their premature failure can be caused by high mechanical stresses or electrical fields. Therefore, it is very important to study the fracture behavior of piezoelectric ceramics under the combined action of mechanical stresses and electrical fields.

Consideration of a crack within the framework of linear fracture mechanics initiates singularities at the crack tips in stresses, deformations and, for piezoelectric materials, in electrical displacements and electric fields. Different ways of removing the crack tip singularities for cracks in homogeneous isotropic materials and modeling of fracture processes were initiated in [Leonov and Panasyuk 1959; Dugdale 1960; Barenblatt 1962].

Important problems of statics and dynamics of structural interfaces, which can be used for an interface crack investigation, were considered in [Bigoni and Movchan 2002; Bertoldi et al. 2007]. The mathematical modeling of the interface crack propagation was carried out in [Peride et al. 2009]. Mode III fracture propagation in prestressed and prepolarized piezoelectric crystals was studied in [Craciun et al. 2004]. Different crack models for interface cracks in piezoelectric bimaterials and in dielectric/piezoelectric ones were investigated in [Li and Chen 2008; Govorukha and Kamlah 2010; Sladek et al. 2012; Xu et al. 2015].

The way of eliminating the electrical displacement singularity for an electrically insulated crack in a homogeneous piezoelectric material was suggested in [Gao and Barnett 1996], due to the development

Keywords: dielectric breakdown model, electrically conductive interface crack, piezoelectric material.

of a polarization saturation (PS) model. It was assumed, similarly to [Dugdale 1960], that the electrical polarization reaches a saturation limit in a line segment in front of the crack. The length of this segment was found from the condition of finiteness of electrical displacement at the end point of the segment. The energy release rate (ERR) for this model was analyzed in [Gao et al. 1997]. A PS model for an electrically permeable crack was studied in [Ru and Mao 1999]. The saturation condition effects on the near-tip field and on the stress intensity factor, as well as the influence of the crack orientation with respect to the electrical polarization direction was investigated in [Ru 1999; Wang 2000] for an electrically impermeable crack. The electric saturation zone of circular and elliptical form in piezoelectric and electrostrictive materials was investigated in [Jeong et al. 2004; Beom et al. 2006a; 2006b]. Different variants of saturation zone for cracks in an interlayer between piezoelectric materials were studied in [Lapusta and Loboda 2009; Loboda et al. 2008; 2010]. A penny-shaped crack in an infinite piezoelectric and thermo-piezo-elastic medium was analyzed with use of PS model in [Fan et al. 2012; Li et al. 2017]. The electric-magnetic polarization saturation model is developed in [Zhao et al. 2015] for the numerical analysis of a nonlinear interfacial crack in three-dimensional transversely isotropic magneto-electro-elastic bimaterial.

The dielectric breakdown (DB) model was developed in [Zhang and Gao 2004], and used to study the problem of an impermeable crack in a piezoelectric material in [Zhang 2004; Zhang et al. 2005]. According to this model the electric field is assumed to be constant and equal to the dielectric breakdown strength in a strip ahead of the crack tip. For a conductive crack the DB model was developed in [Gao et al. 2006] and for a finite sized body it was applied in [Fan et al. 2009] using the boundary element method. The DB model was generalized to the investigation of a conductive crack in an electrostrictive solid in [Zhang and Gao 2012]. Electric and magnetic polarization saturation and breakdown models for penny shaped-cracks in magnetoelectroelastic media were developed in [Zhao et al. 2013]. A semipermeable penny-shaped crack in a piezoelectric media was studied in [Zhao et al. 2016] with use of the DB model. A comparison between the PS and DB models for a penny-shaped cracks in three-dimensional piezoelectric media was performed by [Fan et al. 2014].

It is worth mentioning that all results obtained in the framework of the DB model are related to cracks in homogeneous piezoelectric materials. To the authors' knowledge, no analytical investigations concerning this model have been presented for interface cracks in piezoelectric, piezoelectromagnetic or electrostrictive solids. This can be explained by complexity of the mathematical problem arising in this case. In the present paper the dielectric breakdown model is applied for the first time to the investigation of an interface crack in a piezoelectric bimaterial under anti-plane mechanical and inplane electric loadings. The problem is reduced to the nonhomogeneous combined Dirichlet–Riemann boundary value problem with a special right side. Although this problem appears mathematically more complicated than the Riemann–Hilbert problem, an exact analytical solution is found for an arbitrary length of DB zone. The actual length of this zone is obtained from the condition of electric field finiteness. All required electromechanical quantities are presented in analytical form.

2. Basic equations and motivation for DB model formulation

For a piezoelectric material the relationship between the main electromechanical characteristics are defined by the relations [Parton and Kudryavtsev 1988]

$$\sigma_{ij} = c_{ijks}\varepsilon_{ks} - e_{sij}E_s, \quad D_i = e_{iks}\varepsilon_{ks} + \alpha_{is}E_s,$$

where σ_{ij}, ε_{ij} are the components of stress and strain tensor; D_i, E_i are the components of the electric induction and the electric field, c_{ijks}, e_{sij} are elastic and piezoelectric constants and α_{is} are dielectric constants.

The equilibrium equations in the absence of body forces and free charges are:

$$\sigma_{ij,j} = 0, \quad D_{i,i} = 0.$$

The expressions for the deformation and electric field have the form:

$$\varepsilon_{ij} = \tfrac{1}{2}(u_{i,j} + u_{j,i}), \quad E_i = -\phi_{,i},$$

where u_i are the components of the displacement vector and ϕ is the electric potential.

For the anti-plane mechanical loading and in-plane electric loading assuming the material is transversely isotropic with the poling direction parallel to the x_3-axis one has

$$u_1 = u_2 = 0, \quad u_3 = u_3(x_1, x_2), \quad \phi = \phi(x_1, x_2).$$

Then the constitutive relations can be written in the form

$$\begin{Bmatrix} \sigma_{3i} \\ D_i \end{Bmatrix} = \boldsymbol{R} \begin{Bmatrix} u_{3,i} \\ \phi_{,i} \end{Bmatrix}, \tag{1}$$

where $i = 1, 2$ and $\boldsymbol{R} = \begin{bmatrix} c_{44} & e_{15} \\ e_{15} & -\alpha_{11} \end{bmatrix}$.

The functions u_3 and ϕ satisfy the equations $\Delta u_3 = 0$, $\Delta\phi = 0$; i.e., they are harmonic. Therefore, we present them in the form

$$\boldsymbol{u} = \begin{Bmatrix} u_3 \\ \phi \end{Bmatrix} = 2\,\mathrm{Re}\,\boldsymbol{\Phi}(z) = \boldsymbol{\Phi}(z) + \bar{\boldsymbol{\Phi}}(\bar{z}), \tag{2}$$

where $\boldsymbol{\Phi}(z) = [\Phi_1(z), \Phi_2(z)]^T$ is an arbitrary analytic vector function of the complex variable $z = x_1 + ix_2$ and an upper bar means complex conjugation.

Introducing the vectors

$$\boldsymbol{v}' = [u_3', D_2]^T, \quad \boldsymbol{P} = [\sigma_{32}, -E_1]^T, \tag{3}$$

and substituting (2) in (1) we obtain

$$\boldsymbol{v}' = \boldsymbol{A}\boldsymbol{\Phi}'(z) + \bar{\boldsymbol{A}}\bar{\boldsymbol{\Phi}}'(\bar{z}), \tag{4}$$

$$\boldsymbol{P} = \boldsymbol{B}\boldsymbol{\Phi}'(z) + \bar{\boldsymbol{B}}\bar{\boldsymbol{\Phi}}'(\bar{z}), \tag{5}$$

where

$$\boldsymbol{A} = \begin{bmatrix} 1 & 0 \\ Q_{21} & Q_{22} \end{bmatrix}, \quad \boldsymbol{B} = \begin{bmatrix} Q_{11} & Q_{12} \\ 0 & 1 \end{bmatrix}, \quad \boldsymbol{Q} = i\boldsymbol{R}.$$

Suppose further that the plane (x_1, x_2) is composed of two half-planes $x_1 > 0$ and $x_2 < 0$. The presentation (4), (5) can be written for regions $x_1 > 0$ and $x_2 < 0$ in the form

$$\boldsymbol{v}^{(m)} = \boldsymbol{A}^{(m)}\boldsymbol{\Phi}^{(m)}(z) + \bar{\boldsymbol{A}}^{(m)}\bar{\boldsymbol{\Phi}}^{(m)}(\bar{z}), \quad \boldsymbol{P}^{(m)} = \boldsymbol{B}^{(m)}\boldsymbol{\Phi}'^{(m)}(z) + \bar{\boldsymbol{B}}^{(m)}\bar{\boldsymbol{\Phi}}'^{(m)}(\bar{z}), \tag{6}$$

where $m = 1$ for the upper region and $m = 2$ for the lower one; $\boldsymbol{A}^{(m)}$ and $\boldsymbol{B}^{(m)}$ are the matrices $\boldsymbol{A}$ and $\boldsymbol{B}$ for the regions 1 and 2, respectively; $\boldsymbol{\Phi}^{(m)}(z)$ are arbitrary vector functions, analytic in the regions 1 and 2, respectively. Next we require that the equality $\boldsymbol{P}^{(1)} = \boldsymbol{P}^{(2)}$ holds true on the entire axis x_1. Then it follows from (6) that

$$\boldsymbol{B}^{(1)}\boldsymbol{\Phi}'^{(1)}(x_1 + i0) + \bar{\boldsymbol{B}}^{(1)}\bar{\boldsymbol{\Phi}}'^{(1)}(x_1 - i0) = \boldsymbol{B}^{(2)}\boldsymbol{\Phi}'^{(2)}(x_1 - i0) + \bar{\boldsymbol{B}}^{(2)}\bar{\boldsymbol{\Phi}}'^{(2)}(x_1 + i0). \tag{7}$$

Here $F(x_1 \pm i0)$ designates the limit value of a function $F(z)$ at $x_2 \to 0$ from above or below of the x_1-axis, respectively. The equation (7) can be rewritten as

$$\boldsymbol{B}^{(1)}\boldsymbol{\Phi}'^{(1)}(x_1 + i0) - \bar{\boldsymbol{B}}^{(2)}\bar{\boldsymbol{\Phi}}'^{(2)}(x_1 + i0) = \boldsymbol{B}^{(2)}\boldsymbol{\Phi}'^{(2)}(x_1 - i0) - \bar{\boldsymbol{B}}^{(1)}\bar{\boldsymbol{\Phi}}'^{(1)}(x_1 - i0).$$

The left and right sides of the last equation can be considered as the boundary values of the functions

$$\boldsymbol{B}^{(1)}\boldsymbol{\Phi}'^{(1)}(z) - \bar{\boldsymbol{B}}^{(2)}\bar{\boldsymbol{\Phi}}'^{(2)}(z) \quad \text{and} \quad \boldsymbol{B}^{(2)}\boldsymbol{\Phi}'^{(2)}(z) - \bar{\boldsymbol{B}}^{(1)}\bar{\boldsymbol{\Phi}}'^{(1)}(z), \tag{8}$$

which are analytic in the upper and lower half-planes, respectively. But it means that there is a function $\boldsymbol{M}(z)$, which is equal to the mentioned functions in each half-plane and is analytic in the entire plane.

Assuming that $\boldsymbol{M}(z)|_{z\to\infty} \to 0$, on the basis of the Liouville theorem we find that each of the functions (8) is equal to 0 for any z from the corresponding half-plane. Hence, we obtain

$$\bar{\boldsymbol{\Phi}}'^{(2)}(z) = (\bar{\boldsymbol{B}}^{(2)})^{-1}\boldsymbol{B}^{(1)}\boldsymbol{\Phi}'^{(1)}(z) \quad \text{for } x_2 > 0, \tag{9}$$

$$\bar{\boldsymbol{\Phi}}'^{(1)}(z) = (\bar{\boldsymbol{B}}^{(1)})^{-1}\boldsymbol{B}^{(2)}\boldsymbol{\Phi}'^{(2)}(z) \quad \text{for } x_2 < 0. \tag{10}$$

Further, we find the jump in the vector function

$$\langle \boldsymbol{v}'(x_1)\rangle = \boldsymbol{v}'^{(1)}(x_1 + i0) - \boldsymbol{v}'^{(2)}(x_1 - i0), \tag{11}$$

when passing through the interface. From $(6)_1$ we determine

$$\boldsymbol{v}'^{(m)}(z) = \boldsymbol{A}^{(m)}\boldsymbol{\Phi}'^{(m)}(z) + \bar{\boldsymbol{A}}^{(m)}\bar{\boldsymbol{\Phi}}'^{(m)}(\bar{z}),$$

or

$$\boldsymbol{v}'^{(m)}(x_1 \pm i0) = \boldsymbol{A}^{(m)}\boldsymbol{\Phi}'^{(m)}(x_1 \pm i0) + \bar{\boldsymbol{A}}^{(m)}\bar{\boldsymbol{\Phi}}'^{(m)}(x_1 \mp i0);$$

substituting in (11), one gets

$$\langle \boldsymbol{v}'(x_1)\rangle = \boldsymbol{A}^{(1)}\boldsymbol{\Phi}'^{(1)}(x_1 + i0) + \bar{\boldsymbol{A}}^{(1)}\bar{\boldsymbol{\Phi}}'^{(1)}(x_1 - i0) - \boldsymbol{A}^{(2)}\boldsymbol{\Phi}'^{(2)}(x_1 - i0) - \bar{\boldsymbol{A}}^{(2)}\bar{\boldsymbol{\Phi}}'^{(2)}(x_1 + i0).$$

Finding further $\boldsymbol{\Phi}'^{(2)}(x_1 - i0) = (\boldsymbol{B}^{(2)})^{-1}\bar{\boldsymbol{B}}^{(1)}\bar{\boldsymbol{\Phi}}'^{(1)}(x_1 - i0)$ from (10) and substituting this expression together with (9) in the latest formula at $x_2 \to +0$, leads to

$$\langle \boldsymbol{v}'(x_1)\rangle = \boldsymbol{D}\boldsymbol{\Phi}'^{(1)}(x_1 + i0) + \bar{\boldsymbol{D}}\bar{\boldsymbol{\Phi}}'^{(1)}(x_1 - i0),$$

where $\boldsymbol{D} = \boldsymbol{A}^{(1)} - \bar{\boldsymbol{A}}^{(2)}(\overline{\boldsymbol{B}}^{(2)})^{-1}\boldsymbol{B}^{(1)}$. Introducing a new vector function

$$\boldsymbol{W}(z) = \begin{cases} \boldsymbol{D}\boldsymbol{\Phi}'^{(1)}(z), & x_2 > 0, \\ -\overline{\boldsymbol{D}\boldsymbol{\Phi}'}^{(1)}(z), & x_2 < 0, \end{cases} \tag{12}$$

the last relation can be written as

$$\langle \boldsymbol{v}'(x_1)\rangle = \boldsymbol{W}^{+}(x_1) - \boldsymbol{W}^{-}(x_1), \tag{13}$$

where superscript + and − mean the limit values of $\boldsymbol{W}(z)$ as $z \to x + i0$ and $z \to x - i0$, respectively.

From $(6)_2$ we have

$$\boldsymbol{P}^{(1)}(x_1, 0) = \boldsymbol{B}^{(1)}\boldsymbol{\Phi}'^{(1)}(x_1 + i0) + \bar{\boldsymbol{B}}^{(1)}\bar{\boldsymbol{\Phi}}'^{(1)}(x_1 - i0). \tag{14}$$

It follows from (12) that

$$\boldsymbol{\Phi}'^{(1)}(x_1 + i0) = \boldsymbol{D}^{-1}\boldsymbol{W}(x_1 + i0), \quad \bar{\boldsymbol{\Phi}}'^{(1)}(x_1 - i0) = -(\bar{\boldsymbol{D}}^{-1})^{-1}\boldsymbol{W}(x_1 - i0);$$

substituting these relations into (14) leads to

$$\boldsymbol{P}^{(1)}(x_1, 0) = \boldsymbol{S}\boldsymbol{W}^{+}(x_1) - \bar{\boldsymbol{S}}\boldsymbol{W}^{-}(x_1), \tag{15}$$

where $\boldsymbol{S} = \boldsymbol{B}^{(1)}\boldsymbol{D}^{-1}$. Simple calculations show that

$$\boldsymbol{S} = [\boldsymbol{A}^{(1)}(\boldsymbol{B}^{(1)})^{-1} - \bar{\boldsymbol{A}}^{(2)}(\bar{\boldsymbol{B}}^{(2)})^{-1}]^{-1}. \tag{16}$$

The matrix $\boldsymbol{S}$ for the class of piezoelectric materials being considered has the structure

$$\boldsymbol{S} = \begin{bmatrix} is_{11} & s_{12} \\ s_{21} & is_{22} \end{bmatrix}, \tag{17}$$

where all the s_{kl} are real.

Further transformation of (13) and (15), performed similarly to [Lapusta et al. 2017], leads to

$$\sigma_{32}^{(1)}(x_1, 0) - im_j E_1^{(1)}(x_1, 0) = t_j[F_j^{+}(x_1) + \gamma_j F_j^{-}(x_1)], \tag{18}$$

$$\langle D_2(x_1, 0)\rangle + is_j\langle u_3'(x_1, 0)\rangle = F_j^{+}(x_1) - F_j^{-}(x_1), \tag{19}$$

where

$$F_j(z) = W_2(z) + is_j W_1(z) \quad (j = 1, 2). \tag{20}$$

and

$$s_j = -m_j, \quad t_j = s_{12} - m_j s_{22}, \quad m_j = \mp\sqrt{-\frac{s_{11}s_{12}}{s_{21}s_{22}}}, \quad \gamma_j = -(s_{12} + m_1 s_{22})/t_j \quad (j = 1, 2).$$

Let's assume further that an electrically conductive interface crack arises in the section $[c, a]$ of the material interface. The half-spaces are subjected to uniformly distributed shear stress σ_{23}^{∞} and electric field E_1^{∞} at infinity, which do not depend on coordinate x_3. The crack faces are free of loading. These kinds of external fields produce the anti-plane state, therefore, only the cross-section orthogonal to x_3 (Figure 1) can be considered.

The boundary conditions for the formulated problem for $x_2 = 0$ are

$$\sigma_{23}^{(1)} = \sigma_{23}^{(2)} = 0, \qquad E_1^{(1)} = E_1^{(2)} = 0 \quad \text{for } c < x_1 < a, \tag{21}$$

$$\langle\sigma_{23}\rangle = 0, \quad \langle D_2\rangle = 0, \quad \langle u_3'\rangle = 0, \quad \langle E_1\rangle = 0 \quad \text{for } x_1 \notin (c, a). \tag{22}$$

Satisfying conditions (21) and (22) with the use of (18), (19) for $j = 1$ provide the continuity of the function $F_1(z)$ over the segments $x_1 \notin (c, a)$ of the material interface and also leads to

$$F_1^{+}(x_1) + \gamma_1 F_1^{-}(x_1) = 0 \quad \text{for } c < x_1 < a. \tag{23}$$

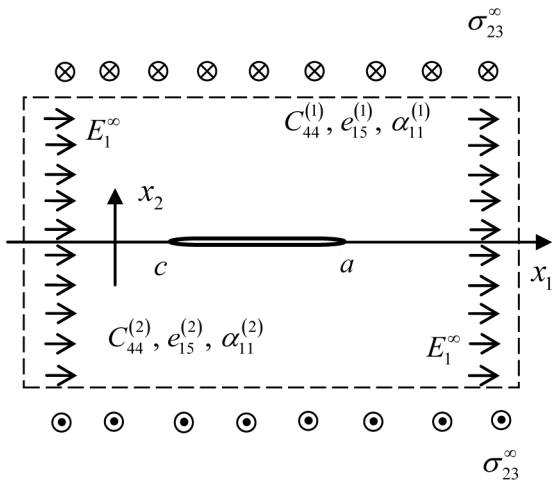

Figure 1. An electrically conducting crack between two piezoelectric materials.

Taking into account further that for $x_1 \notin (c, a)$ the relationships $F_1^+(x_1) = F_1^-(x_1) = F_1(x_1)$ are valid, it follows from (18) that

$$(1+\gamma_1)t_1 F_1(x_1) = \sigma_{23}^{(1)}(x_1, 0) - im_1 E_1^{(1)}(x_1, 0) \quad \text{as } x_1 \to \infty.$$

Using that the function $F_1(z)$ is analytic in the whole plane cut along (c, a) and applying the conditions at infinity, one gets from the last equation

$$F_1(z)|_{z\to\infty} = \tilde{\sigma}_{23} - i\tilde{E}_1, \tag{24}$$

where $\tilde{\sigma}_{23} = \sigma_{23}^{\infty}/r_1,\ \tilde{E}_1 = m_1 E_1^{\infty}/r_1,\ r_1 = (1+\gamma_1)t_1$.

The solution of (23) under the condition at infinity (24) was found with use of [Muskhelishvili 1977] in the form

$$F_1(z) = (\tilde{\sigma}_{23} - i\tilde{E}_1)\frac{z - (a+c)/2 - i\varepsilon l}{\sqrt{(z-c)(z-a)}}\left(\frac{z-c}{z-a}\right)^{i\varepsilon}, \tag{25}$$

where $\varepsilon = \frac{1}{2\pi}\ln\gamma_1$, $l = a - c$.

A similar analysis can be carried out for $j = 2$ in (18), (19) and the function $F_2(z)$ can be obtained.

The stress and electric fields at the interface are obtained from (18), (25) as follows:

$$\sigma_{23}^{(1)}(x_1, 0) - im_1 E_1^{(1)}(x_1, 0) = \pm(\sigma_{23}^{\infty} - im_1 E_1^{\infty})\frac{x_1 - (a+c)/2 - i\varepsilon l}{\sqrt{(x_1-c)(x_1-a)}}\left(\frac{x_1-c}{x_1-a}\right)^{i\varepsilon} \text{ for } x_1 > a, \tag{26}$$

where the upper sign corresponds to $x_1 > a$ and the lower sign to $x_1 < c$.

The electric induction and the derivative of the displacement jumps are found from the formula (19) in the form

$$\langle D_2(x_1, 0)\rangle + is_1\langle u_3'(x_1, 0)\rangle = -\frac{(\sigma_{23}^{\infty} i + m_1 E_1^{\infty})}{t_1\sqrt{\gamma_1}}\frac{(x_1 - (a+c)/2 - i\varepsilon l)}{\sqrt{(x_1-c)(a-x_1)}}\left(\frac{x_1-c}{a-x_1}\right)^{i\varepsilon} \text{ for } c < x_1 < a. \tag{27}$$

Integrating the last relation, we obtain

$$\langle \hat{D}_2(x_1,0)\rangle + is_1\langle u_3(x_1,0)\rangle = \sqrt{(x_1-c)(a-x_1)}\left\{\frac{\sigma_{23}^{\infty} i + m_1 E_1^{\infty}}{t_1\sqrt{\gamma_1}}\left(\frac{x_1-c}{a-x_1}\right)^{i\varepsilon}\right\} \quad \text{for } c < x_1 < a, \quad (28)$$

where $\langle \hat{D}_2(x_1,0)\rangle = \int \langle D_2(x_1,0)\rangle dx_1$.

It should be noted that for the case of a homogeneous material formulas (26) and (28) take the form

$$\sigma_{23}^{(1)}(x_1,0) - im_1 E_1^{(1)}(x_1,0) = \pm(\sigma_{23}^{\infty} - im_1 E_1^{\infty})\frac{x_1-(a+c)/2}{\sqrt{(x_1-c)(x_1-a)}} \quad \text{for} \begin{cases} x_1 > a \ (+\text{ sign}), \\ x_1 < c \ (-\text{ sign}), \end{cases} \quad (29)$$

$$\langle \hat{D}_2(x_1,0)\rangle + is_1\langle u_3(x_1,0)\rangle = t_1^{-1}(\sigma_{23}^{\infty} i + m_1 E_1^{\infty})\sqrt{(x_1-c)(a-x_1)} \quad \text{for } c < x_1 < a. \quad (30)$$

It is clearly seen from the formulas (29), (30) that mechanical and electrical components are independent for a homogeneous material, therefore, electrical characteristics at the whole interface are completely defined by external electric loading while mechanical – by mechanical one. Another situation takes place when considering the case of a bimaterial treated here. In this case mechanical and electrical components are coupled (see Equations (26)–(30)) and their mutual influence is demonstrated in Figures 2–5.

The calculations were performed for a bimaterial with the following characteristics:

$$c_{44}^{(1)} = 35.3\,\text{GPa}, \quad e_{15}^{(1)} = 17.0\ \text{C/m}^2, \quad \alpha_{11}^{(1)} = 15.1\times 10^{-9} \quad \text{C/(Vm)},$$
$$c_{44}^{(2)} = 42.5\,\text{GPa}, \quad e_{15}^{(2)} = -0.48\,\text{C/m}^2, \quad \alpha_{11}^{(2)} = 0.0757\times 10^{-9}\,\text{C/(Vm)},$$

and different values of mechanical and electric loadings.

The calculated tangential crack openings (sliding) $\langle u_3(x_1,0)\rangle$ for $c = -10$ mm, $b = 10$ mm, $\sigma_{23}^{\infty} = 10$ MPa, and different values of E_1^{∞} are presented in Figure 2 for the right vicinity of the left crack tip and for the left vicinity of the right tip. It is seen that for $E_1^{\infty} = 0$ the crack opening has the same behavior, but with different values of sliding, at the left and right crack tips. However an increase of E_1^{∞} leads to increasing the crack opening at the left crack tip and decreasing it at the right one.

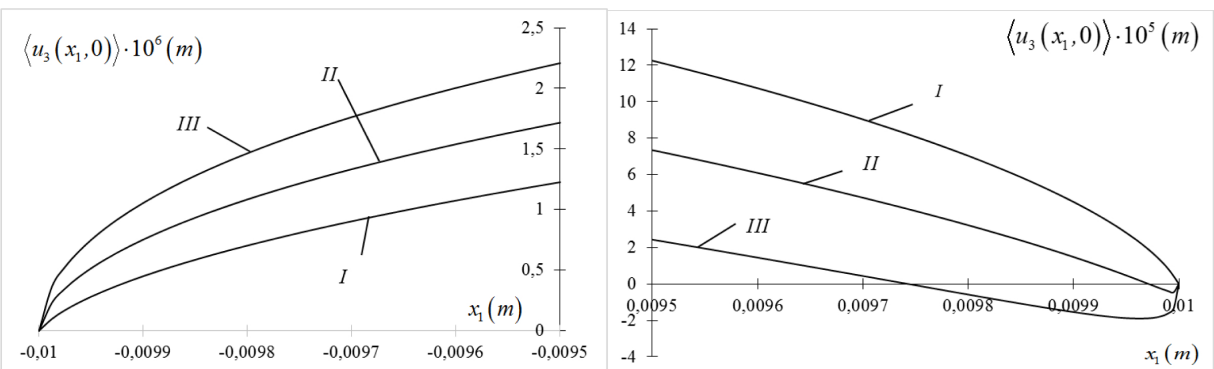

Figure 2. Dependence of the crack sliding $\langle u_3(x_1,0)\rangle$ at the left and right crack tips, respectively, on E_1^{∞} for $\sigma_{23}^{\infty} = 10$ MPa. Curves *I*, *II* and *III* correspond to $E_1^{\infty} = 0$, 300 kV/m and 600 kV/m, respectively.

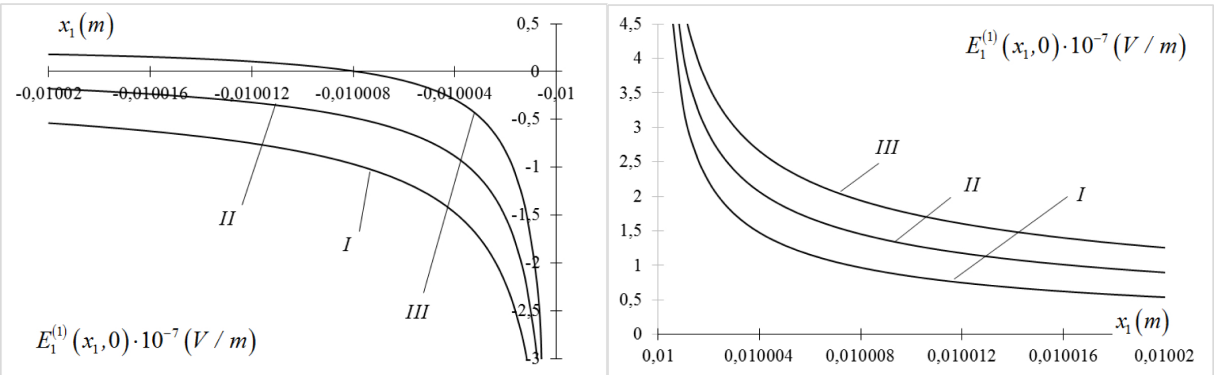

Figure 3. Variation of the electric field $E_1^{(1)}(x_1, 0)$ along the left crack continuation (left) and the right crack continuation for $\sigma_{23}^{\infty} = 10\,\text{MPa}$ and different values of E_1^{∞}.

The variation in electric field $E_1^{(1)}(x_1, 0)$ along the crack continuations for the same materials, crack length and loadings are given in Figure 3. These figures suggest that an increase in E_1^{∞} causes an increase in the intensity of the electric field at the right crack tip and a decrease in its absolute value at the left crack tip. Changing the E_1^{∞} sign leads to the same phenomenon, but with permutation of the crack tips. Thus, in contrast to the case of a crack in a homogeneous material, the electrical fields at the right and left crack tips of an interface crack become substantially different for nonzero external electric fields.

In some cases it is necessary to know the behavior of electromechanical quantities outside of the material interface. To define this behavior we obtain from $(6)_2$ and (12)

$$\boldsymbol{P}^{(m)} = 2\,\text{Re}\{\boldsymbol{K}^{(m)}\,\boldsymbol{W}(z)\}, \tag{31}$$

where $\boldsymbol{K}^{(1)} = \boldsymbol{B}^{(1)}\boldsymbol{D}^{-1}$, $\boldsymbol{K}^{(2)} = -\boldsymbol{B}^{(2)}\bar{\boldsymbol{D}}^{-1}$.

Considering $j = 1$ and $j = 2$ in (20) and solving the system obtained with respect to $W_1(z)$ and $W_2(z)$ one gets

$$W_1(z) = \frac{F_1(z) - F_2(z)}{i(s_1 - s_2)}, \qquad W_2(z) = \frac{s_2 F_1(z) - s_1 F_2(z)}{s_2 - s_1} \tag{32}$$

Formulas (31) and (32) define the shear stress and the electric field component at any point of the bimaterial domain via the functions $F_1(z)$ and $F_2(z)$ obtained above.

Figure 4 demonstrates the result of use of the formulas (31) and (32) for determination and presentation of electromechanical characteristics outside of the material interface. Namely, the shear stress distribution at the right crack tip in the upper part of the medium is shown in this figure. The curves with markers represent the level lines of the shear stress $\sigma_{32}^{(1)}(x_1, 0)$, which demonstrate its variation in the vicinity of the right crack tip. Similar fields can be drawn with use of (31) and (32) for other electromechanical components at any subdomain of the medium.

3. Formulation of the problem and dielectric breakdown model consideration for an interface crack

By separating the real and imaginary parts of (26) one can see that the mechanical stress and the electric

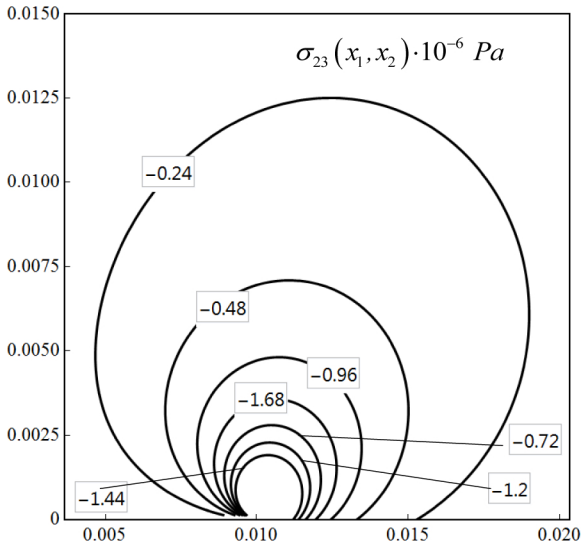

Figure 4. Variation of the shear stress $\sigma_{23}(x_1, x_2)$ distribution at the vicinity $0.004\,m \leq x_1 \leq 0.02\,m$, $0 \leq x_2 \leq 0.015\,m$ of the right crack tip.

field are singular at the crack tips. Moreover this singularity is oscillating. Square root singularity takes place at the crack tip also in a case of a homogeneous material. To remove the oscillation and to eliminate completely the singularity in the electric field the dielectric breakdown model (DB model) is applied. This model was suggested in papers by [Zhang and Gao 2004] for a conducting crack in a homogeneous piezoelectric material. In the present paper the generalization of this model to the interface crack is suggested. As follows from Figures 2 and 3, the DB zone lengths should be different at the left and right tips of an interface crack. Moreover, it will be shown later that these zones for an interface crack are either both very short (for $E_1^{\infty} = 0$) or one zone is substantially shorter than another one, therefore, their mutual influence can be neglected. Taking into account this circumstance we'll consider for simplicity only one zone paying the main attention to the longer one and assuming that it occurs at the right crack tip (Figure 5). If the longer zone occurs at another crack tip then this zone can be considered by simple transformation of half-spaces.

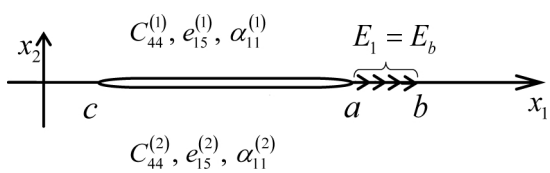

Figure 5. An electrically conducting interface crack with dielectric breakdown zone at the right crack tip.

Thus the boundary conditions for the considered model can be written as

$$\sigma_{23}^{(1)} = \sigma_{23}^{(2)} = 0, \quad E_1^{(1)} = E_1^{(2)} = 0 \text{ for } c < x_1 < a, \tag{33}$$

$$E_1^{(1)} = E_1^{(2)} = E_b, \quad \langle \sigma_{23} \rangle = 0, \quad \langle u_3' \rangle = 0, \text{ for } a < x_1 < b, \tag{34}$$

$$\langle \sigma_{23} \rangle = 0, \quad \langle D_2 \rangle = 0, \quad \langle u_3' \rangle = 0, \langle E_1 \rangle = 0 \text{ for } x_1 \notin (c, b), \tag{35}$$

where E_b is the dielectric breakdown strength, defined as a critical electric field at which partial discharge starts to occur around the crack tip [Gao et al. 2006].

Satisfying the interface conditions (33) with use of (18) one gets the equation (23), and the first and third conditions (34) together with (19) lead to

$$\begin{aligned} &\operatorname{Im}[F_1^+(x_1) + \gamma_1 F_1^-(x_1)] = -m_1 E_b / t_1, \\ &\operatorname{Im}[F_1^+(x_1) - F_1^-(x_1)] = 0 \text{ for } a < x_1 < b. \end{aligned} \tag{36}$$

Satisfaction of the boundary conditions (35) provides the analyticity of the function $F_1(z)$ outside of the interval (c, b). The relations (36) lead to the equation

$$\operatorname{Im} F_1^{\pm}(x_1) = E^* \text{ for } a < x_1 < b, \tag{37}$$

where $E^* = -m_1 E_b / r_1$.

Equations (23) and (37) present the nonhomogeneous combined Dirichlet–Riemann boundary value problem. The conditions at infinity (24) remain valid for this problem also. Following the paper by [Nakhmein and Nuller 1986] the general solution of the homogeneous problem corresponding to (23), (37) can be presented in the form

$$F_{1h}(z) = P(z) X_1(z) + Q(z) X_2(z), \tag{38}$$

where

$$P(z) = C_1 z + C_2, \quad Q(z) = D_1 z + D_2.$$

The functions

$$X_1(z) = i e^{i\chi(z)} / \sqrt{(z-c)(z-b)}, \quad X_2(z) = e^{i\chi(z)} / \sqrt{(z-c)(z-a)}, \tag{39}$$

are the canonical solutions of the homogeneous problem corresponding to (23), (37),

$$\chi(z) = 2\varepsilon \ln \frac{\sqrt{(b-a)(z-c)}}{\sqrt{(b-a)(z-a)} + \sqrt{(a-c)(z-b)}}, \quad z = x_1 + i\, x_2,$$

$i = \sqrt{-1}$ and $C_1,\ C_2,\ D_1,\ D_2$ are arbitrary real coefficients.

A particular solution of the nonhomogeneous problem (23), (37) we'll find in the form

$$F_{1p}(z) = \Phi(z) X_1(z), \tag{40}$$

where $\Phi(z)$ is assumed to be analytic in the whole complex plane with a cut $[a,\ b]$ along the x_1-axis. It is obvious that $F_{1p}(z)$ satisfies (23). Substituting (40) into (37) and taking into account that $\operatorname{Im} X_1^{\pm}(x_1) = 0$ on $(a,\ b)$ one gets the following equation

$$\operatorname{Im} \Phi^{\pm}(x_1) = \psi^{\pm}(x_1) \text{ for } a < x_1 < b, \tag{41}$$

where $\psi(x_1) = E^*/X_1(x_1)$.

A solution of the Dirichlet problem (41) has the following form [Gakhov 1966, formula (46.25)]:

$$\Phi(z) = \frac{Y(z)}{2\pi}\int_a^b \frac{\psi^+(t)+\psi^-(t)}{Y^+(t)(t-z)}\,dt + \frac{1}{2\pi}\int_a^b \frac{\psi^+(t)-\psi^-(t)}{t-z}\,dt, \tag{42}$$

where $Y(z) = \sqrt{(z-a)(z-b)}$ and $0 \le \arg(z-a) \le 2\pi$, $0 \le \arg(z-b) \le 2\pi$.

Taking into account that

$$\psi^+(t)+\psi^-(t) = -2E^*\sqrt{(t-c)(b-t)}\sinh\chi_0(t),$$
$$\psi^+(t)-\psi^-(t) = 2E^*\sqrt{(t-c)(b-t)}\cosh\chi_0(t),$$
$$\chi_0(x_1) = 2\varepsilon\tan^{-1}\sqrt{\frac{(a-c)(b-x_1)}{(b-c)(x_1-a)}}$$

and that $Y^+(t) = -i\sqrt{(t-a)(b-t)}$ on (a,b), the formula (42) takes the form

$$\Phi(z) = \frac{E^*}{\pi}[-iY(z)L_1(z) + L_2(z)], \tag{43}$$

where

$$L_1(z) = \int_a^b \sqrt{\frac{t-c}{t-a}}\,\frac{\sinh\chi_0(t)}{t-z}\,dt, \quad L_2(z) = \int_a^b \sqrt{(t-c)(b-t)}\,\frac{\cosh\chi_0(t)}{t-z}\,dt.$$

The general solution of the problem (23), (37) is the sum of the solutions (38), (40). Arbitrary constants C_1, C_2, D_1, D_2 can be found from the condition at infinity (24) together with condition of the displacement uniqueness and the absence of an electric charge in the crack region [Knysh et al. 2012], which due to (8) can be written in the form

$$\int_c^b (F_1^+(x_1) - F_1^-(x_1))dx_1 = 0.$$

Taking into account that for the validity of last equation the coefficient before z^{-1} in the expansion of $F_1(z)$ at infinity should be equal to zero [Herrmann and Loboda 2003] and also

$$X_1(z)|_{z\to\infty} = iz^{-2}e^{i\beta}\left(z + i\beta_1 + \frac{c+b}{2}\right) + o(z^{-3}),$$
$$X_2(z)|_{z\to\infty} = z^{-2}e^{i\beta}\left(z + i\beta_1 + \frac{c+a}{2}\right) + o(z^{-3}),$$
$$\Phi(z)|_{z\to\infty} = -iR + o(z^{-1}), \quad R = \frac{E^*}{\pi}\int_a^b \sqrt{\frac{t-c}{t-a}}\sinh\chi_0(t)\,dt,$$

one gets the following expressions for the unknown coefficients

$$C_1 = -\tilde{\sigma}_{23}\sin\beta - \tilde{E}_1\cos\beta, \quad D_1 = \tilde{\sigma}_{23}\cos\beta - \tilde{E}_1\sin\beta,$$
$$C_2 = -\frac{c+b}{2}C_1 - \beta_1 D_1, \quad D_2 = \beta_1 C_1 - \frac{c+a}{2}D_1 - R,$$

where

$$\beta = \varepsilon \ln \frac{1-\sqrt{1-\lambda}}{1+\sqrt{1-\lambda}}, \beta_1 = \varepsilon\sqrt{(a-c)(b-c)}, \quad \lambda = \frac{b-a}{b-c}. \tag{44}$$

From the exact analytical solution thus obtained,

$$F_1(z) = (P(z) + \Phi(z))X_1(z) + Q(z)X_2(z), \tag{45}$$

all required quantities at the material interface can be found. A similar analysis can be carried out for $j = 2$ in (18), (19), leading to the function $F_2(z)$.

4. Stress intensity factor and DB zone length

According to equation (18) stress and electric field on the right hand side from DB zone can be presented in the form

$$\sigma_{32}^{(1)}(x_1, 0) - im_1 E_1^{(1)}(x_1, 0) = r_1 F_1(x_1) = r_1\{(P(x_1) + \Phi(x_1))X_1(x_1) + Q(x_1)X_2(x_1)\}. \tag{46}$$

For an arbitrary position of the point b (defining the DB zone length) right hand side of (46) is singular for $x_1 \to b+0$ and besides $P(b) + \Phi(b)$ is real and $X_1(x_1)|_{x_1 \to b+0} = i/\sqrt{(b-c)(x_1-b)}$ is pure imaginary. Therefore, for any b the shear stress $\sigma_{32}^{(1)}(x_1, 0)$ is finite for $x_1 \to b+0$ whilst $E_1^{(1)}(x_1, 0)$ is singular. To remove this singularity the equation

$$P(b) + \Phi(b) = 0$$

should be satisfied. After some transformation this equation can be written in the form

$$m_1 E_1^{\infty} \cos\beta + \sigma_{23}^{\infty} \sin\beta + 2\varepsilon\sqrt{1-\lambda}(\sigma_{23}^{\infty} \cos\beta - m_1 E_1^{\infty} \sin\beta) - \frac{2m_1 E_b}{\pi(b-c)} \int_a^b \sqrt{\frac{t-c}{b-t}} \cosh\chi_0(t)\, dt = 0. \tag{47}$$

The obtained equation should be solved with respect to λ and then the point b can be found from the last of (44). As a rule (47) can be solved numerically and the largest root of this equation from the interval $(0,\ 1)$, which we denote λ_0, can be found.

In the particular case of homogeneous piezoelectric material one has $\varepsilon = 0$, $\chi_0(t) = 0$, $\beta = 0$, and equation (47) reduces to the form

$$\frac{2}{\pi(b-c)} \int_a^b \sqrt{\frac{t-c}{b-t}}\, dt = \frac{E_1^{\infty}}{E_b}.$$

After some transformations this can be written as

$$\frac{\sqrt{\lambda}}{\pi} \int_{-1}^{1} \sqrt{\frac{2+\lambda(\tau+1)}{1-\tau}} d\tau = \frac{E_1^{\infty}}{E_b}. \tag{48}$$

For a small λ this equation has the following asymptotic solution

$$\lambda \approx \lambda_0 = \left(\frac{\pi E_1^{\infty}}{4E_b}\right)^2. \tag{49}$$

For the case of two symmetrical DB zones $(-b, -a)$ and (a, b) at both crack tips in a homogeneous piezoelectric material the analysis similar to [Gao et al. 2006] leads to the following equation

$$\frac{a}{b} = \cos\frac{\pi E_1^\infty}{2E_b}. \tag{50}$$

Note that the asymptotic solution of this equation for small E_1^∞/E_b completely coincides with the solution (49).

The shear stress at (a, b) according to (18), (34) can be found in the form

$$\sigma_{32}^{(1)}(x_1, 0) = t_1[F_1^+(x_1) + \gamma_1 F_1^-(x_1)] + im_1 E_b.$$

Substituting the formula (45), taking into account that according to [Herrmann and Loboda 2003]

$$X_1^\pm(x_1) = \frac{\pm e^{\pm\chi_0(x_1)}}{\sqrt{(x_1-c)(b-x_1)}}, \quad X_2^\pm(x_1) = \frac{e^{\pm\chi_0(x_1)}}{\sqrt{(x_1-c)(x_1-a)}} \text{ for } x_1 \in (a, b)$$

and applying Plemeli's formulas [Muskhelishvili 1977] we arrive at the expression

$$\begin{aligned} t_1^{-1}\sigma_{32}^{(1)}(x_1, 0) = {} & P(x_1)\frac{e^{\chi_0(x_1)} - \gamma_1 e^{-\chi_0(x_1)}}{\sqrt{(x_1-c)(b-x_1)}} + Q(x_1)\frac{e^{\chi_0(x_1)} + \gamma_1 e^{-\chi_0(x_1)}}{\sqrt{(x_1-c)(x_1-a)}} \\ & + \frac{E^*}{\pi}\left\{-\sqrt{\frac{x_1-a}{x_1-c}}[e^{\chi_0(x_1)} + \gamma_1 e^{-\chi_0(x_1)}]L_1(x_1) + \frac{e^{\chi_0(x_1)} - \gamma_1 e^{-\chi_0(x_1)}}{\sqrt{(x_1-c)(b-x_1)}}L_2(x_1)\right\}, \end{aligned} \tag{51}$$

where the integrals $L_1(x_1)$ and $L_2(x_1)$ should be considered in sense of principal value on Cauchy [Muskhelishvili 1977].

Consider next the stress intensity factor (SIF) of the shear stress at the point a

$$K_3 = \lim_{x_1 \to a+0} \sqrt{2\pi(x_1-a)}\, \sigma_{23}^{(1)}(x_1, 0). \tag{52}$$

Taking into account that $L_1(x_1)$ has a square root singularity for $x_1 \to a+0$ and $L_2(x_1)$ has the logarithmic singularity at this point we arrive to the following formula

$$K_3 = 2t_1\sqrt{2\pi\gamma_1}\frac{Q(a)}{\sqrt{a-c}},$$

which after some transformations takes the form

$$K_3 = \frac{2t_1\sqrt{2\pi\gamma_1}}{\sqrt{a-c}}\left[\frac{b-c}{2}\sqrt{1-\lambda}(2\varepsilon C_1 + \sqrt{1-\lambda}D_1) - R\right]. \tag{53}$$

In the particular case of homogeneous piezoelectric material formula (53) reduces to

$$K_3 = \sqrt{\frac{\pi(a-c)}{2}}\sigma_{23}^\infty,$$

which completely coincides with the associated result of [Gao et al. 2006].

The derivative of the crack faces displacement jump at the interval (c, a) (crack sliding) can be found with use of (8) in the form

$$\langle u_3'(x_1, 0)\rangle = s_1^{-1}\,\mathrm{Im}[F_1^+(x_1) - F_1^-(x_1)].$$

$10^{-6}E_1^{\infty}$ [V/m]	0	1	2	3	4	5
λ_0	2.492×10^{-4}	7.285×10^{-3}	0.02571	0.05521	0.0947	0.1429
$10^{-6}K_3$ [Pa/m$^{3/2}$]	1.514	0.3850	−0.3448	−0.8656	−1.2375	−1.4879

Table 1. DB-zone length and SIF K_3 for $\sigma_{23}^{\infty} = 10$ MPa and different positive values of E_1^{∞}

$10^{-6}E_1^{\infty}$ [V/m]	−0.1	−0.2	−1	−2
λ_0	1.078×10^{-4}	3.522×10^{-5}	1.055×10^{-9}	2.419×10^{-11}
$10^{-6}K_3$ [Pa/m$^{3/2}$]	1.6739	1.852	4.061	7.531

Table 2. DB-zone length and SIF K_3 for $\sigma_{23}^{\infty} = 10$ MPa and different negative values of E_1^{∞}.

Substituting expression (31) one gets

$$\langle u_3'(x_1,0)\rangle = \frac{\gamma_1+1}{s_1\sqrt{\gamma_1}}\,\mathrm{Im}\left\{\left[\frac{P(x_1)+\Phi(x_1)}{\sqrt{b-x_1}} - i\frac{Q(x_1)}{\sqrt{a-x_1}}\right]\frac{\exp[i\chi^*(x_1)]}{\sqrt{x_1-c}}\right\} \text{ for } c<x_1<a, \tag{54}$$

where

$$\chi^*(x_1) = 2\varepsilon \ln \frac{\sqrt{(b-a)(x_1-c)}}{\sqrt{(b-c)(a-x_1)}+\sqrt{(a-c)(b-x_1)}}$$

and the crack sliding can be found as

$$\langle u_3(x_1,0)\rangle = \int_c^{x_1} \langle u_3'(t,0)\rangle\, dt. \tag{55}$$

5. Numerical results and discussion

We performed calculations for a bimaterial composed of PZT-4 (upper material) and $BaTiO_3$ (lower one) having the following characteristics:

$$c_{44}^{(1)} = 25.6\,\text{GPa}, \quad e_{15}^{(1)} = 12.7\,\text{C/m}^2, \quad \alpha_{11}^{(1)} = 6.46\,\text{nC(V m)}^{-1},$$
$$c_{44}^{(2)} = 43.0\,\text{GPa}, \quad e_{15}^{(2)} = 11.6\,\text{C/m}^2, \quad \alpha_{11}^{(2)} = 11.2\,\text{nC(V m)}^{-1},$$

with $E_b = 10^7\,\frac{\text{V}}{\text{m}}$ [Fan et al. 2009], $c = -10$ mm, $b = 10$ mm and different values of mechanical and electric loadings.

In Table 1 the DB zone lengths and the SIF K_3 are presented for $\sigma_{23}^{\infty} = 10$ MPa and different positive values of E_1^{∞}. It can be seen from the results that increasing of E_1^{∞} leads to the increase of λ_0 and decrease of K_3 with resulting in its change of sign even. The reason for the change will be clear from the following graphs. Similar results, but for negative values of E_1^{∞} are presented in Table 2. It follows from this table that increasing of $|E_1^{\infty}|$ initiates the cardinal decreasing of the DB zone length to negligibly small values.

Results similar to Table 1, but for smaller values of σ_{23}^{∞}, are presented in Table 3. It is seen by comparison of these Tables that increase of σ_{23}^{∞} leads to an increase of λ_0 and K_3. However with increase of E_1^{∞} the difference in λ_0 for these two Tables almost disappear.

$10^{-6}E_1^\infty$ [V/m]	0	1	2	3	4	5
λ_0	8.036×10^{-5}	6.537×10^{-3}	0.0247	0.05412	0.09363	0.14188
$10^{-6}K_3$ [Pa/m$^{3/2}$]	0.7264	−0.4672	−1.211	−1.738	−2.113	−2.3659

Table 3. DB-zone length and SIF K_3 for $\sigma_{23}^\infty = 5$ MPa and different positive values of E_1^∞.

$10^{-6}E_1^\infty$ [V/m]	1	2	3	4	5
λ_0	6.144×10^{-4}	0.02428	0.05660	0.09295	0.1410
$\hat{\lambda}$	6.156×10^{-4}	0.02447	0.05449	0.09549	0.1464

Table 4. DB-zone lengths in case of homogenous material $BaTiO_3$ for $\sigma_{23}^\infty = 10$ MPa and different values of E_1^∞.

The results for the DB zone lengths in case of homogenous material $BaTiO_3$ for $\sigma_{23}^\infty = 10$ MPa and different values of E_1^∞ are given in Table 4. Value λ_0 in this case is the root of (48) corresponding to one DB zone and $\hat{\lambda}$ is the root of (50) obtained for two symmetrical DB-zones at both crack tips. The SIF K_3 for all values of E_1^∞ is equal to 1.772×10^6 Pa/m$^{3/2}$. It is clear that for relatively small magnitudes of E_1^∞ the difference between λ_0 and $\hat{\lambda}$ is negligibly small, but it grows moderately as E_1^∞ increases.

The calculated tangential crack opening (sliding) $\langle u_3(x_1, 0)\rangle$ for $c = -10$ mm, $b = 10$ mm, $\sigma_{23}^\infty = 10$ MPa is presented in Figure 6 for different values of E_1^∞. Lines *I*, *II* and *III* correspond to $E_1^\infty = 0$, 2×10^6 V/m and 4×10^6 V/m, respectively. It is clearly seen from these results that the crack sliding is almost symmetrical for $E_1^\infty = 0$, but increasing of E_1^∞ leads to the distortion of the curve and a change of the sign of $\langle u_3(x_1, 0)\rangle$ in a region in the vicinity of the right crack tip (these explain the negative values of SIF in Table 1). However, the appearance of the negative $\langle u_3(x_1, 0)\rangle$ does not mean the crack faces interpenetration like in plane case and is quite admissible from physical point of view. It is worth to be mentioning also that the negative electric field will lead to mirror mapping of the obtained graphs with respect to the ordinate axis.

The behavior of the electric field in the DB zone and along its right continuation are presented in Figure 7 for the same crack geometry, mechanical loading and different E_1^∞. Here $E_1^\infty = 2 \times 10^6$ V/m (line *I*), 4×10^6 V/m (*II*) and 5×10^6 V/m (*III*). As it can be seen the DB-model eliminated the singularities of electric field at the right crack tip. Thus this model gives the possibility to get an electromechanical field at the point b free from singularities and to transform the oscillating singularity of the shear stress into conventional square root singularity at the point a. It is very important because it provides a possibility for the SIF to be used in a conventional way.

For an additional verification of the obtained analytical solution the independent methods based on finite element package has been used. The finite sized body composed of two piezoelectric parallelepipeds $-30\,\text{mm} \le x_1 \le 30\,\text{mm}$, $0 \le x_2 \le 20\,\text{mm}$, $0 \le x_3 \le 180\,\text{mm}$ and $-30\,\text{mm} \le x_1 \le 30\,\text{mm}$, $-20\,\text{mm} \le x_2 \le 0$, $0 \le x_3 \le 180\,\text{mm}$ with the same piezoelectric material parameters as presented at the beginning of this Section has been considered. An electrically conducting crack in the interface region $-10\,\text{mm} \le x_1 \le 10\,\text{mm}$, $x_2 = 0$, $0 \le x_3 \le 180\,\text{mm}$ is situated. The lower boundary $x_2 = -20$ mm was fixed while to the upper one $x_2 = 20$ mm the uniformly distributed shear stress $\sigma_{32}^{(1)}(x_1,20) = 10$ MPa was applied. Assuming the external electric field $E_1 = 0$ the DB zone in this case is defined by the second column of Table 1.

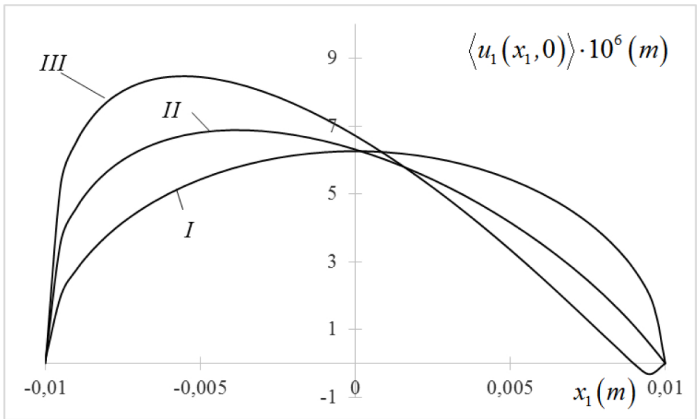

Figure 6. Tangential crack sliding $\langle u_3(x_1, 0)\rangle$ for $\sigma_{23}^{\infty} = 10\,\text{MPa}$ and different values of E_1^{∞}.

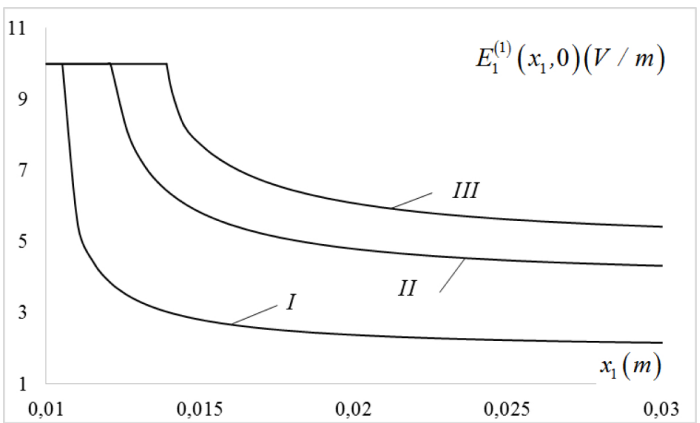

Figure 7. The electric field in DB zone and at it continuation for $\sigma_{23}^{\infty} = 10\,\text{MPa}$ and different values of E_1^{∞}.

The finite element ABAQUS code was used for the solution of this problem. The mesh refinement at the crack tips was done. As a result of this solution the maximum value of the crack sliding at the point $x_1 = x_2 = 0$, $x_3 = 90\,\text{mm}$ turned out to be $6.771 \times 10^{-3}\,\text{mm}$. Analytical analysis performed for the same geometrical and mechanical parameters gave the result $6.260 \times 10^{-3}\,\text{mm}$ for the crack sliding at the same point. Taking into account that we compared the results for finite size domain (with a crack 3 times shorter than the width of the compound) and for an infinite domain, the obtained error in 7.54% can be considered as quite satisfactory. Therefore, the presented numerical analysis confirms the validity of the analytical approach developed in this paper.

6. Conclusions

The mode III interface crack problem for a transversely isotropic dissimilar piezoelectric bimaterial media under the action of anti-plane mechanical loading and in-plane electrical field parallel to the crack faces is considered.

To eliminate the electric field singularity, which occurs at the crack tips, the dielectric breakdown model is applied. According to this model the electric field along some zone of the crack continuation is assumed to be equal to the electric breakdown strength E_b and the length of this zone remain unknown for a time being. A nonhomogeneous combined Dirichlet–Riemann boundary value problem (23), (37) is formulated. This problem is much more complicated than the problem (23) nevertheless an exact analytical solution (45) of this problem is presented. The transcendental equation for the determination of the DB zone length is obtained from the condition of the electric field finiteness at the boundary point of this zone. Analytical formulas for the shear stress in DB zone, the stress intensity factor at the crack tip and for the crack sliding are obtained.

The variation of the DB zone length, crack sliding and the SIF with respect to external electric field is illustrated in tables and figures. In particular it is shown that the electric field essentially influences all electrical and also mechanical characteristics of the model. Namele, the increase of the electric field changes the sign of the displacement jump in some part of the crack region (see line *III* of Figure 5). It is seen from the last lines of Tables 1 and 3 that this increase cardinally vary the value of the SIF changing it sign even.

The particular case of identical physical properties of upper and lower domains is considered. This case is equivalent to the case of a crack in a homogeneous piezoelectric medium. Equation (47), determining the DB zone length, and the formula (53) for the SIF finding reduce to very simple equations which solutions are in good agreement with the associated results obtained for the crack with two DB zones by another method.

It's worth to be mentioning that the dissimilarity of the bulk properties essentially effects the electromechanical quantities of the considered problem. In particular, the SIF K_3 does not depend on the applied electric field for a homogeneous case whilst it changes its value quite substantially with respect to this field for a dissimilar piezoelectric material. Besides, as it is seen from Figure 6, the crack opening transforms its symmetrical form due to electric field for a dissimilar material what is not observed for a homogeneous one.

Comparison of the obtained analytical solution with the associated results obtained by finite element method has been performed and good agreement has been found.

The importance of the obtained solution is justified by the possibility of using the obtained results in electronic engineering for decreasing of the threat of failure of electronic devices produced from dissimilar piezoelectric materials and having internal electrodes, which can lead to the appearance of conducting interface cracks.

Acknowledgments

This work was sponsored by a public grant overseen by the French National Research Agency as part of the "Investissements d'Avenir" through the IMobS3 Laboratory of Excellence (ANR-10-LABX-0016) and through the IDEX-ISITE initiative CAP 20-25 (ANR-16-IDEX-0001) within the framework of the program WOW PhD Mentoring.

References

[Barenblatt 1962] G. I. Barenblatt, "The mathematical theory of equilibrium cracks in brittle fracture", *Adv. Appl. Mech.* **7** (1962), 55–129.

[Beom et al. 2006a] H. G. Beom, Y. H. Kim, C. Cho, and C. B. Kim, "A crack with an electric displacement saturation zone in an electrostrictive material", *Arch. Appl. Mech.* **76** (2006a), 19–31.

[Beom et al. 2006b] H. G. Beom, Y. H. Kim, C. Cho, and C. B. Kim, "Asymptotic analysis of an impermeable crack in an electrostrictive material subjected to electric loading", *Int. J. Solids Struct.* **43** (2006b), 6869–6886.

[Bertoldi et al. 2007] K. Bertoldi, D. Bigoni, and W. J. Drugan, "Structural interfaces in linear elasticity, part I: Nonlocality and gradient approximations", *J. Mech. Phys. Solids* **55** (2007), 1–34.

[Bigoni and Movchan 2002] D. Bigoni and A. B. Movchan, "Statics and dynamics of structural interfaces in elasticity", *Int. J. Solids Struct.* **39** (2002), 4843–4865.

[Craciun et al. 2004] E.-M. Craciun, E. Baesu, and E. Soós, "General solution in terms of complex potentials for incremental antiplane states in prestressed and prepolarized piezoelectric crystals: application to mode III fracture propagation", *IMA J. Appl. Math.* **70** (2004), 39–52.

[Dugdale 1960] D. S. Dugdale, "Yielding of steel sheets containing slits", *J. Mech. Phys. Solids* **8** (1960), 100–108.

[Fan et al. 2009] C. Y. Fan, M. H. Zhao, and Y. H. Zhou, "Numerical solution of polarization saturation/ dielectric breakdown model in 2D finite piezoelectric media", *J. Mech. Phys. Solids* **57** (2009), 1527–1544.

[Fan et al. 2012] C. Y. Fan, Y. F. Zhao, M. H. Zhao, and E. Pan, "Analytical solution of a semi-permeable crack in a 2D piezoelectric medium based on the PS model", *Mech. Res. Commun.* **40** (2012), 34–40.

[Fan et al. 2014] C. Y. Fan, Z. H. Guo, H. Y. Dang, and M. H. Zhao, "Extended displacement discontinuity method for nonlinear analysis of penny-shaped cracks in three-dimensional piezoelectric media", *Eng. Anal. Bound. Elem.* **38** (2014), 8–16.

[Gakhov 1966] F. D. Gakhov, *Boundary value problems*, Pergamon Press, 1966.

[Gao and Barnett 1996] H. Gao and D. M. Barnett, "An invariance property of local energy release rate in a strip saturation model of piezoelectric fracture", *Int. J. Fract.* **79** (1996), R25–R29.

[Gao et al. 1997] H. Gao, T. Y. Zhang, and P. Tong, "Local and global energy release rates for an electrically yielded crack in a piezoelectric ceramic", *J. Mech. Phys. Solids* **45** (1997), 491–510.

[Gao et al. 2006] C. F. Gao, N. Noda, and T. Y. Zhang, "Dielectric breakdown model for a conductive crack and electrode in piezoelectric materials", *Int. J. Eng. Sci.* **44:3–4** (2006), 256–272.

[Govorukha and Kamlah 2010] V. Govorukha and M. Kamlah, "On contact zone models for an electrically limited permeable interface crack in a piezoelectric bi-material", *Int. J. Fract.* **164(1)** (2010), 133–146.

[Herrmann and Loboda 2003] K. P. Herrmann and V. V. Loboda, "Fracture mechanical assessment of interface cracks with contact zones in piezoelectric bimaterials under thermoelectromechanical loadings, I: Electrically permeable interface cracks", *Int. J. Solids Struct.* **40** (2003), 4191–4217.

[Jeong et al. 2004] K. M. Jeong, I. O. Kim, and H. G. Beom, "Effect of electric displacement saturation on the stress intensity factor for a crack in a ferroelectric ceramic", *Mech. Res. Comm.* **31** (2004), 371–382.

[Knysh et al. 2012] P. Knysh, V. Loboda, F. Labesse-Jied, and Y. Lapusta, "An electrically charged crack in a piezoelectric material under remote electromechanical loading", *Lett. Fract. Micromech.* **175**:1 (2012), 87–94.

[Lapusta and Loboda 2009] Y. Lapusta and V. Loboda, "Electro-mechanical yielding for a limited permeable crack in an interlayer between piezoelectric materials", *Mech. Res. Commun.* **36** (2009), 183–192.

[Lapusta et al. 2017] Y. Lapusta, O. Onopriienko, and V. Loboda, "An interface crack with partially electrically conductive crack faces under antiplane mechanical and in-plane electric loadings", *Mech. Res. Commun.* **81** (2017), 38–43.

[Leonov and Panasyuk 1959] M. Y. Leonov and V. V. Panasyuk, "Development of the smallest cracks in a rigid body", *Appl. Mech.* **5:4** (1959), 391–401.

[Li and Chen 2008] Q. Li and H. Chen, "Solution for a semi-permeable interface crack in elastic dielectric/piezoelectric bimaterials", *J. Appl. Mech.* (*ASME*) **75(1)** (2008), 011010.

[Li et al. 2017] P.-D. Li, X.-Y. Li, G.-Z. Kang, C.-F. Gao, and R. Müller, "Crack tip electric polarization saturation of a thermally loaded penny-shaped crack in an infinite thermo-piezo-elastic medium", *Int. J. Solids Struct.* **117** (2017), 67–79.

[Loboda et al. 2008] V. Loboda, Y. Lapusta, and V. Govorukha, "Mechanical and electrical yielding for an electrically insulated crack in an interlayer between piezoelectric materials", *Int. J. Eng. Sci.* **46** (2008), 260–272.

[Loboda et al. 2010] V. Loboda, Y. Lapusta, and A. Sheveleva, "Limited permeable crack in an interlayer between piezoelectric materials with different zones of electric saturation and mechanical yielding", *Int. J. Solids Struct.* **47** (2010), 1796–1806.

[Muskhelishvili 1977] N. I. Muskhelishvili, *Some basic problems of mathematical theory of elasticity*, Noordhoff, 1977.

[Nakhmein and Nuller 1986] E. L. Nakhmein and B. M. Nuller, "Contact between an elastic half-plane and a partly separated stamp", *J. Appl. Math. Mech.* **50**:4 (1986), 507–515.

[Parton and Kudryavtsev 1988] V. Z. Parton and B. A. Kudryavtsev, *Electromagnetoelasticity*, Gordon and Breach Science Publishers, 1988.

[Peride et al. 2009] N. Peride, A. Carabineanu, and E.-M. Craciun, "Mathematical modelling of the interface crack propagation in a pre-stressed fiber reinforced elastic composite", *Comput. Mater. Sci.* **45(1)** (2009), 684–692.

[Ru 1999] C. Q. Ru, "Effect of electrical polarization saturation on stress intensity factors in a piezoelectric ceramics", *Int. J. Solids Struct.* **36** (1999), 869–883.

[Ru and Mao 1999] C. Q. Ru and X. Mao, "Conducting crack in a piezoelectric ceramics of limited electrical polarization", *J. Mech. Phys. Solids* **47** (1999), 2125–2146.

[Sladek et al. 2012] J. Sladek, V. Sladek, M. Wnsche, and C. Zhang, "Analysis of an interface crack between two dissimilar piezoelectric solids", *Eng. Fract. Mech.* **89** (2012), 114–117.

[Wang 2000] T. C. Wang, "Analysis of strip electric saturation model of crack problem in piezoelectric materials", *Int. J. Solids Struct.* **37** (2000), 6031–6049.

[Xu et al. 2015] C. H. Xu, Z. H. Zhou, X. S. Xu, and A. Y. T. Leung, "Electroelastic singularities and intensity factors for an interface crack in piezoelectric-elastic bimaterials", *Appl. Math. Model.* **39**:9 (2015), 2721–2739.

[Zhang 2004] T. Y. Zhang, "Dielectric breakdown model for an electrical impermeable crack in a piezoelectric material", *Comput. Mater. Continua* **1** (2004), 107–115.

[Zhang and Gao 2004] T. Y. Zhang and C. F. Gao, "Fracture behavior of piezoelectric materials", *Theor. Appl. Fract. Mech.* **41** (2004), 339–379.

[Zhang and Gao 2012] N. Zhang and C. F. Gao, "Effects of electrical breakdown on a conducting crack or electrode in electrostrictive solids", *Eur. J. Mech. A Solids* **32** (2012), 62–68.

[Zhang et al. 2005] T. Y. Zhang, M. H. Zhao, and C. F. Gao, "The strip dielectric breakdown model", *Int. J. Fract.* **132** (2005), 311–327.

[Zhao et al. 2013] M. H. Zhao, Z. H. Guo, C. Y. Fan, and E. Pan, "Electric and magnetic polarization saturation and breakdown models for penny shaped cracks in 3D magnetoelectroelastic media", *Int. J. Solids Struct.* **50** (2013), 1747–1754.

[Zhao et al. 2015] Y. F. Zhao, M. H. Zhao, and E. Pan, "Displacement discontinuity analysis of a nonlinear interfacial crack in three-dimensional transversely isotropic magneto-electro-elastic bi-materials", *Eng. Anal. Bound. Elem.* **61** (2015), 254–264.

[Zhao et al. 2016] M. Zhao, H. Dang, G. Xu, and C. Fan, "Dielectric breakdown model for an electrically semi-permeable penny-shaped crack", *Acta Mech. Solida Sin.* **29**:5 (2016), 536–546.

Received 15 Jun 2019. Revised 11 Nov 2019. Accepted 15 Nov 2019.

YURI LAPUSTA: yuri.lapusta@sigma-clermont.fr
Université Clermont Auvergne, CNRS, SIGMA Clermont, Institut Pascal, F-63000 Clermont-Ferrand, France

ALLA SHEVELEVA: allasheveleva@i.ua
Department of Theoretical and Computational Mechanics, Oles Honchar Dnipro National University, Dnipro, 49010, Ukraine

FRÉDÉRIC CHAPELLE: frederic.chapelle@sigma-clermont.fr
Université Clermont Auvergne, CNRS, SIGMA Clermont, Institut Pascal, F-63000 Clermont-Ferrand, France

VOLODYMYR LOBODA: loboda@dnu.dp.ua
Department of Theoretical and Computational Mechanics, Oles Honchar Dnipro National University, Dnipro, 49010, Ukraine

JOURNAL OF MECHANICS OF MATERIALS AND STRUCTURES

msp.org/jomms

Founded by Charles R. Steele and Marie-Louise Steele

Cover photo: Ev Shafrir

See msp.org/jomms for submission guidelines.

JoMMS (ISSN 1559-3959) at Mathematical Sciences Publishers, 798 Evans Hall #6840, c/o University of California, Berkeley, CA 94720-3840, is published in 10 issues a year. The subscription price for 2020 is US $660/year for the electronic version, and $830/year (+$60, if shipping outside the US) for print and electronic. Subscriptions, requests for back issues, and changes of address should be sent to MSP.

JoMMS peer-review and production is managed by EditFLOW® from Mathematical Sciences Publishers.

PUBLISHED BY

mathematical sciences publishers

nonprofit scientific publishing

http://msp.org/

Journal of Mechanics of Materials and Structures

Volume 15, No. 1 January 2020

Stress-minimizing holes with a given surface roughness in a remotely loaded elastic plane SHMUEL VIGDERGAUZ and ISAAC ELISHAKOFF 1

Analytical modeling and computational analysis on topological properties of 1-D phononic crystals in elastic media MUHAMMAD and C. W. LIM 15

Dynamics and stability analysis of an axially moving beam in axial flow YAN HAO, HULIANG DAI, NI QIAO, KUN ZHOU and LIN WANG 37

An approximate formula of first peak frequency of ellipticity of Rayleigh surface waves in an orthotropic layered half-space model TRUONG THI THUY DUNG, TRAN THANH TUAN, PHAM CHI VINH and GIANG KIEN TRUNG 61

Effect of number of crowns on the crush resistance in open-cell stent design GIDEON PRAVEEN KUMAR, KEPING ZUO, LI BUAY KOH, CHI WEI ONG, YUCHENG ZHONG, HWA LIANG LEO, PEI HO and FANGSEN CUI 75

A dielectric breakdown model for an interface crack in a piezoelectric bimaterial YURI LAPUSTA, ALLA SHEVELEVA, FRÉDÉRIC CHAPELLE and VOLODYMYR LOBODA 87

Thermal buckling and free vibration of Timoshenko FG nanobeams based on the higher-order nonlocal strain gradient theory GORAN JANEVSKI, IVAN PAVLOVIĆ and NIKOLA DESPENIĆ 107

A new analytical approach for solving equations of elasto-hydrodynamics in quasicrystals VALERY YAKHNO 135

Expansion-contraction behavior of a pressurized porohyperelastic spherical shell due to fluid redistribution in the structure wall VAHID ZAMANI and THOMAS J. PENCE 159